



HAL
open science

Impact of chemical exchange on transverse relaxation at low and moderate magnetic field strengths for sugar solutions representative of fruit tissues analyzed by simulation and MRI experiments

Rodolphe Leforestier, François Mariette, Maja Musse

► To cite this version:

Rodolphe Leforestier, François Mariette, Maja Musse. Impact of chemical exchange on transverse relaxation at low and moderate magnetic field strengths for sugar solutions representative of fruit tissues analyzed by simulation and MRI experiments. *Journal of Magnetic Resonance*, 2021, 322, pp.106872. 10.1016/j.jmr.2020.106872 . hal-03139305

HAL Id: hal-03139305

<https://hal.inrae.fr/hal-03139305>

Submitted on 18 Sep 2023

HAL is a multi-disciplinary open access archive for the deposit and dissemination of scientific research documents, whether they are published or not. The documents may come from teaching and research institutions in France or abroad, or from public or private research centers.

L'archive ouverte pluridisciplinaire **HAL**, est destinée au dépôt et à la diffusion de documents scientifiques de niveau recherche, publiés ou non, émanant des établissements d'enseignement et de recherche français ou étrangers, des laboratoires publics ou privés.

TITLE: Impact of chemical exchange on transverse relaxation at low and moderate magnetic field strengths for sugar solutions representative of fruit tissues analyzed by simulation and MRI experiments

Authors: Rodolphe Leforestier, François Mariette, Maja Musse

INRAE UR OPAALE, 17, rue de Cucillé, 35044 Rennes France.

Corresponding author: Maja MUSSE

Address : 17 avenue de Cucillé, CS 64427, 35044 Rennes, France

Telephone : +33223482179

E-mail : maja.musse@inrae.fr

SUMMARY

Proton exchange effects on transverse relaxation rate were studied at low and moderate magnetic fields. Analysis was conducted on low-concentrate simple sugar (fructose and glucose) solutions modeling the vacuolar liquid in fruits. Simulated data obtained from Carver and Richards equations were used to analyze the effects of temperature and pH on parameters involved in the chemical exchange mechanisms. The results have highlighted that measurement conditions and tissue characteristics (echo time, magnetic field strength, temperature, pH, etc.) significantly impact the transverse relaxation rate via chemical exchange, even for low and mid magnetic fields and the narrow echo time ranges of TD-NMR and MRI measurements. This explains some of the divergent relaxation data from plant tissue NMR measurements reported in the literature and emphasizes the importance of taking experimental conditions and tissue characteristics into account when interpreting results. It also clearly demonstrates that the appropriate choice of experimental conditions can emphasize the effects of sugar concentration or pH variations on transverse relaxation in vacuolar liquids, making it possible to monitor these parameters accurately via transverse relaxation measurements. The impact of concentration, solute type, pH and temperature on transverse relaxation of sugar solutions were demonstrated experimentally at 1.5T with an MRI scanner. These data were interpreted using the Carver–Richards model which was effective in estimating parameters involved in chemical exchange mechanism in the imaging experiment.

Key words: Magnetic Resonance Imaging, Time Domain Nuclear Magnetic Resonance, NMR transverse relaxation, fruit, chemical exchange, CPMG dispersion curve, fructose, glucose

1. INTRODUCTION

Time Domain (TD) NMR and MRI relaxometry are suitable for the characterization of plant tissues [1] as they make it possible to access information on the status and distribution of water at cell and tissue levels. A number of applications of these techniques in plant and food science have been reported on various issues, such as fruit or leaf development [2, 3], storage of fruits and tubers [4] and drying and freezing processes [5]. Although valuable insights into the changes in tissue characteristics have been obtained, interpretation of the variations in relaxation parameters that occur during these processes remains a complex task. This is due to the multiple changes in composition and structure that a plant tissue undergoes during its transformation (composition, cell size, pH, etc.), and to the impact of these changes on the relaxation parameters via different physical and chemical mechanisms which, in turn, depend on the experimental conditions (magnetic field strength and experimental protocol). As a result, dissociating the different relaxation mechanisms in plant tissue is far from straightforward. Indeed, the transverse relaxation mechanisms can be considered by representing the plant cells in the first approximation as several water pools with different bulk T_2 relaxation. In each pool, the bulk relaxation is mainly defined by proton exchanges between water and cell metabolites and membranes. At the cell and tissue levels, the relatively slow diffusive exchange between water pools through semi-permeable membranes, gives rise to a multi exponential signal that reflects water compartmentalization. As a consequence of the diffusion exchanges, the observed T_2 of water pools depends on compartment size and membrane properties. Finally, the presence of air-filled intercellular spaces in plant tissues may also affect observed relaxation times due to differences between the magnetic susceptibility of air and water [1].

As a consequence of the complexity of the relaxation mechanisms in plant tissues, a number of divergent results are reported in the literature. One typical example concerns fruit drying studied by TD NMR. For example, dehydration of apple samples resulting in a 45% mass reduction in one case strongly reduced ($\sim 50\%$) the T_2 of the vacuolar water [6] (20MHz, TE=5.6ms), while it did not produce any effect on the vacuolar water transverse relaxation in [5] (100MHz, TE=0.4ms). For higher mass losses ($\sim 50\%$), vacuolar T_2 decreased for about 50% and 20% in apple [5] and broccoli [7] (23.3MHz, TE=33ms) tissues respectively, while it remained unchanged in tomato ([8]; 20MHz, TE=0.2ms). Some opposite results were also observed during fruit maturation. During the maturation of kiwi [2] (85MHz, TE=20ms) no impact on the mono-exponential T_2 relaxation times measured by MRI was observed, despite an increase in dry matter and sugar concentration of 68% and 200% respectively. By contrast, during the postharvest ripening of banana [9], the T_2 of all components of the multi-exponential signal measured by TD-NMR increased (20MHz, TE=2ms). Finally, TD-NMR studies showed that a temperature increase in apple resulted in the increase in the T_2 of the vacuole water [5](100MHz,

TE=0.4ms), while the opposite was observed in potato [10] (23.2 MHz, TE=0.3ms). The above examples suggest that variations in the T_2 of vacuolar water probably often reflect several physical and chemical phenomena that are simultaneously altered by the process under investigation.

In the vacuole, one of the main phenomena related to bulk water relaxation is proton exchange between water and cell metabolites. The contribution of proton exchange depends on the concentration and transverse relaxation of exchangeable solute protons, the chemical shift ($\Delta\omega$) between protons from different molecular environments involved in the exchange, and on the exchange rate (k_b). The last is modulated by temperature and the pH of the medium [11], whereas $\Delta\omega$ depends on solute (sugars and organic acids) structure and on magnetic field intensity. The impact of chemical exchange on the T_2 value also depends on the pulse spacing of the Carr-Purcell-Meiboom-Gill (CPMG) sequence, as the ratio between the pulse spacing and the exchange rate determines the dephasing of the spins from different molecular environments. This effect, which gives rise to a dispersion phenomenon, is described by the Carver-Richards model [12].

Although the effect of chemical exchanges on transverse relaxation in plant tissues strongly depend on experimental conditions, they were mainly investigated at relatively high magnetic fields of 100MHz and above [13, 14], while the magnetic fields ranging between 20 and 100MHz have rarely been investigated. Moreover, these investigations concern TD NMR while in MRI studies, the impact of chemical exchanges on T_2 has often been overlooked and the changes in T_2 with echo time have been mostly attributed to the effects of magnetic susceptibility induced by tissue porosity. In order to address these two issues, the work presented in this paper focuses primarily on the understanding at low to moderate magnetic fields (0.2 to 1.5T) of mechanism involved in chemical exchange impacting the bulk transverse relaxation times of liquids in plant tissues. In the first step, numerical simulations based on the Carver and Richards model (Appendix A) were used to explore the impact of magnetic field strength on the observed T_2 , by taking into consideration the pulse space ranges used in MRI and TD NMR experiments. The range of the magnetic field strengths analyzed corresponded to that of TD-NMR spectrometers and MR imaging systems usually used for plant applications. Then, the impact of temperature and pH on chemical exchanges effects and consequently on the observed T_2 values was investigated. The study was performed on systems that simulated vacuole liquid, corresponding to the solution of small molecules (fructose and glucose), with small chemical shifts (0.8-1.2ppm) and low concentrations (with no changes in viscosity). The aim was to demonstrate how a slight variation in experimental conditions (magnetic field strength, pulse spacing, temperature, pH) will impact the transverse relaxation times measured in the conditions of TD NMR or MRI experiments. In a second step, the impact of temperature, concentration, solute type and pH on T_2 of sugar solutions were analyzed experimentally at 1.5T with an MRI scanner. The Carver and Richards model was successful

in analyzing the dispersion curves obtained by MRI, despite the constraints of the imaging experiment (range of relatively long TE used, inhomogeneities in B_1 and B_0 , imperfect refocusing pulses, etc).

2. MATERIALS AND METHODS

NUMERICAL SIMULATION

Sets of simulated T_2 -dispersion curves for aqueous solutions of sugars were generated with Scilab 5 software (Scilab, ESI Group, France). The effects of magnetic field intensity (B_0) on the T_2 -dispersion curves were studied at 8, 20, 60, 80, 100 and 200MHz (0.2, 0.5, 1.5, 1.9, 2.4 and 4.7T, respectively) corresponding to a range of TD NMR spectrometers and MR imaging systems usually used for plant applications. The dispersion curves were generated with TE spanning the range of values generally used in TD NMR (0.1-10ms; 40 values equally spaced on a logarithmic scale) and imaging (6.5-20ms; 10 values equally spaced on a logarithmic scale) relaxometry experiments. P_b was fixed to 0.015, which corresponds to the ratio of the number of sugar hydroxyl groups to the total number of hydroxyl groups in fructose or glucose 60g/L solution. The sugar molecular structure was taken into account by setting the differences in chemical shift between water and sugar protons at 0.8 and 1.2 ppm for fructose and glucose respectively [15]. The effects of temperature (Eyring's law, Eq.1) and pH (Eq.2) on the T_2 of sugar solutions were studied respectively by varying the exchange rate k_b [11, 16]:

$$k_b = \frac{K_B T}{h} \exp\left(\frac{-\Delta G}{RT}\right) \quad \text{Eq. 1}$$

$$k_b = k_1 [H_3O^+] + k_2 K_w / [H_3O^+] \quad \text{Eq.2}$$

where K_B is the Boltzmann constant, h the Planck constant, ΔG the Gibbs energy of activation, R the gas constant, k_1 and k_2 are the exchange rate constants of the acid-base reaction, and K_w is the autoprotolysis constant for water. T_{2a} was set to the relaxation time of pure water, measured experimentally for different temperatures, while T_{2b} was fixed at 50ms which corresponds approximately to the relaxation times of the non-exchangeable protons of simple sugars in dilute systems [17]. Variations in T_{2b} and $\Delta\omega$ were considered to be negligible across the temperature range (8-32°C) and for the low sugar concentrations studied according to [18].

EXPERIMENTAL

Samples

D-glucose and D-fructose were purchased from Sigma Chemicals and used as such without further purification. The solutions were obtained by dissolving sugars in ultra-pure water (resistivity at 25°C: 18.2 MΩ.cm, Synergy UV Water Purification System, Merck, Darmstadt, Germany) and adding

sodium azide (2.0 mmol/L) as the antibacterial agent, under constant stirring. The pH was adjusted to selected values at 7.0 and 4.4 with sodium hydroxide and hydrochloric acid respectively, purchased from Sigma Chemicals.

The experimental setup involved seven 50mL tubes (3.4 cm in diameter and 7.0 cm in height) containing different solutions: 1) pure water; 2) 29.4g/L fructose, pH=4.4; 3) 29.4g/L fructose, pH=7.0; 4) 28.8g/L glucose, pH=4.4; 5) 28.8g/L glucose, pH=7.0; 6) 14.7g/L fructose+14.4g/L glucose, pH=4.4 and 7) 29.4g/L fructose+28.8g/L glucose, pH=4.4. The tubes were placed on a specially designed base with 2mm thick neoprene pads between the tubes and the base to prevent vibrations.

Magnetic Resonance Imaging

MRI measurements were performed on a 1.5T scanner (Magnetom Avanto, Siemens, Erlangen, Germany) equipped with a circular polarized head array coil. The prepared apparatus was placed in a temperature regulating device installed inside the RF coil. Five optical fibers connected to a data logger (UMI8, FISO Technologies Inc., Canada) were inserted into the tubes and used to control the temperature of the solutions during the MRI experiment. Prior to the experiment, the uncertainty of the temperature measurement was estimated to be less than 1°C.

T₂ was measured using a multi spin echo (MSE) sequence [19] with 256 echoes and the first echo (TE) equal to the inter-echo spacing. The parameters common to all experiments were: transverse orientation, Field Of View 152x152mm², matrix size 128x128, slice thickness 5mm, pixel bandwidth 260Hz, Repetition Time 10s and 1 scan. Experiments were performed at 8, 12, 15, 20, 24, 28 and 32°C with TE set at 6.5, 7, 8, 9, 10, 12, 14, 16, 18 and 20ms.

Regions of interest (ROI) for each tube were selected with ImageJ software (National Institutes of Health, USA). The signal was then averaged for each ROI and for all the MSE magnitude images of the series. The signal to noise ratio (SNR) was obtained by taking the ratio of the mean signal in the image to the mean signal in the background divided by $\sqrt{\frac{\pi}{2}}$. Only data characterized by a SNR greater than 7 were kept for relaxation parameter estimation, making it possible to assume zero-mean Gaussian noise distribution in magnitude images at all echo times [20]. Mono-exponential T₂ values were obtained by fitting the relaxation curves using the Levenberg-Marquardt algorithm with TableCurve 2D Software (Systat Software Inc., USA).

The repeatability of the T₂ measurements, including acquisition and image processing steps, was estimated by acquiring three scans at TE=6.5ms with independent scanner settings (automatic frequency and transmitter attenuation/gain adjustments and shimming) at four different temperatures (8, 15, 24 and 32°C). In all cases, the standard deviation of the three repetitions was less than 0.4% of the T₂ value measured in each tube.

Estimation of the Carver and Richards NMR parameters

The dispersion curves of each experimental condition studied consisted of 8 T_2 measurements at different TE values (from 6.5 to 16ms). The fitting of the experimental dispersion curve with the two-site expression of Carver and Richards model was carried out using the Levenberg-Marquardt algorithm implemented in the Datafit function of Scilab 5 software. The outputs of the fit were: k_b , $\Delta\omega$ and T_{2b} , while, T_{2a} was fixed at the value measured for pure water at each temperature. After a first adjustment at the lowest temperature (8°C) where all the parameters were estimated (P_b , k_b , $\Delta\omega$ and T_{2b}), it was confirmed that the estimated value of P_b was close to its theoretical value corresponding to the ratio of the number of sugar hydroxyl groups to the total number of hydroxyl groups in the solution. P_b was then fixed at the value of this preliminary adjustment.

Due to experimental constraints, the TE values could not be chosen optimally, the minimum value being 6.5ms. As a consequence, the estimation of the parameters from the adjustment on the experimental data was an ill-posed inverse problem that depended on the initial guess. Fitting was therefore stabilized by first estimating the initial guess through the direct mapping of the parameter space [21]. This consisted in the comparison of the experimental T_2 values ($T_{2,exp}$) with those calculated at the points of a multidimensional grid ($T_{2,theo}$) delimiting a space of physically reasonable parameters for k_b , $\Delta\omega$ and T_{2b} . The grid was defined as followed (minimum; maximum; step) using values from the literature: k_b in s^{-1} (200; 3000; 10), $\Delta\omega$ in ppm (0.7; 1.3; 0.0025) and T_{2b} in s (0.01; 0.05; 0.0005). The combination with the lowest sum of the squares of the differences between ($T_{2,exp}$) and ($T_{2,theo}$) was selected as the initial guess. The dispersion curves were then fitted as a function of the pulse spacing for different temperatures i.e. 8, 11, 15, 20 and 24°C.

3. RESULTS AND DISCUSSION

SIMULATED DATA

Numerical simulations of the effects of magnetic field strength and exchange rates on the dispersion curves for sugar aqueous solutions at low (8 (0.2T) and 20MHz (0.5T)), mid (60 (1.5T) and 80 MHz (1.9T)) and relatively high (100 (2.3T) and 200MHz (4.7T)) magnetic field strengths are shown in Fig.1. A more detailed analysis of the complex effects of temperature on T_2 of sugar solutions was then carried out for low and mid magnetic field ranges (i.e. 20 and 60MHz) where the effects of chemical exchanges have generally been considered to be minor and for the echo times (1, 6.5 and 14ms) representative of the TD-NMR and MRI experiments on plants (Fig. 2). The temperature range from 5 to 40°C was analyzed, as it corresponds to that encountered in physical processes where the integrity of the cell is preserved. An analysis of the effects of sugar concentration, sugar type and pH

on T_2 of sugar solutions is given in Appendix B (Fig B 1-3). In both Fig. 2 and Appendix B, data were systematically compared with data corresponding to the well-described dispersion curves at 100MHz reported by Hills et al. [13].

Effect of magnetic field strength

Fig. 1 depicts the dispersion curves for a general case simulating the vacuolar compartment of fleshy fruit parenchyma (glucose concentration of 60g/L; 96% water content) for exchange rates of $300s^{-1}$ (Fig. 1A) and $1000s^{-1}$ (Fig. 1B), corresponding approximately to temperatures of 5 and 20°C respectively and neutral pH [22]. Considering the two figures, both the effects of the exchange rate and the magnetic field on the dispersion curves can be observed. The characteristic shape of the dispersion curves shows a decrease in transverse relaxation rate (R_2) with TE^{-1} between two plateaus observed for the long and short TE values. According to the Swift and Connick equations [13, 23], T_2 values at the plateaus for long (Eq.3) and short TE (Eq.4) respectively are expressed as follows:

$$R_2 = \frac{1}{T_{2a}} + \frac{P_b k_b}{P_a} \left\{ \frac{T_{2b}^{-2} + T_{2b}^{-1} k_b + \Delta\omega^2}{(T_{2b}^{-1} + k_b)^2 + \Delta\omega^2} \right\} \quad \text{Eq. 3}$$

$$R_2 = \frac{P_a}{T_{2a}} + \frac{P_b}{T_{2b} + k_b^{-1}} \quad \text{Eq.4}$$

showing that for long TEs the relaxation rate increases with the exchange rate and with the magnetic field strength (Fig. 1 A and B), and also with the difference in chemical shifts (Eq.3), while at short echo times (Eq.4) the R_2 is independent of the field strength.

Differences in regimes should be taken into account considering the ratio between the chemical exchange rate and the difference in the chemical shifts between the two spin populations for each of the two k_b analyzed. In the case of $k_b=300s^{-1}$ (Fig. 1A), slow exchange regime ($k_b \ll \Delta\omega$) with the mid-point at $TE^{-1}=\Delta\omega/2$ is effective for magnetic fields $\geq 80\text{MHz}$, while a transition between slow and fast exchange regimes can be observed for $B_0 > 100\text{MHz}$. For this value of k_b , no fast exchange regime condition is observed for the TE and B_0 ranges investigated. In the case of a higher exchange rate with $k_b=1000s^{-1}$ (Fig. 1B) the fast exchange regime ($k_b \gg \Delta\omega$) with the mid-point at $TE^{-1}=k_b/2$ is only effective for magnetic fields $\leq 80\text{MHz}$. Where k_b is $300s^{-1}$ or $1000s^{-1}$, the dispersion curves at fields below and over 80MHz correspond to an intermediate regime where k_b is close to $\Delta\omega$. For $k_b=300s^{-1}$ (Fig. 1 A), in the pulse spacing range from 0.1ms to 20ms R_2 increases only slightly, from 0.94 to $1.04s^{-1}$ (T_2 1.06 and 0.96s) at 8MHz, while it markedly increases from 0.94 to $1.51s^{-1}$ (T_2 1.06 and 0.66s) and from 0.94 to

3.50s^{-1} (T_2 1.06 and 0.29s) at 20 and 60MHz respectively. This effect is pronounced by increasing k_b from 300 to 1000s^{-1} (Fig. 1 B).

It should be pointed out that a significant variation in R_2 can be observed (Fig. 1) even for mid field strengths and for the range of small TE variations observed in MRI experiments (6.5 to 20ms) because the conditions of the long TE limit which depend on the ratio $k_b/\Delta\omega$ are not reached. A transition of the system between slow and fast exchange regimes makes it complex to analyze the impact of magnetic field on R_2 dispersion effects. Interestingly, in the range of MRI TE values (6.5-20ms), for $k_b=300\text{s}^{-1}$ (Fig. 1A), the strongest relative variation in R_2 occurs at 60MHz (about 25%) while it is relatively low at 100 and 200MHz (~5%). For $k_b=1000\text{s}^{-1}$ (Fig. 1B), the strongest variation in R_2 also occurs at 60MHz while, unlike the previous case, it is very similar for 80 and 100MHz. As might be expected, for the echo time range used in TD-NMR relaxometry (0.1-6ms), the relative increase in R_2 with echo time is modulated by the magnetic field. Note that for a moderate magnetic field of 1.5T (60MHz), the variation in TE between 0.1 and 2ms induces an increase in R_2 of around 30%, reaching up to 60% for $TE>3\text{ms}$. The condition of the short TE limit is reached for $TE<0.1\text{ms}$ for all cases, except for 200MHz and $k_b=1000\text{s}^{-1}$.

Effects of temperature

Fig. 2 depicts the complex impact of temperature (5-40°C) on the relaxation rate for a 20g/L glucose solution and neutral pH at 20, 60 and 100MHz and for different echo times (1, 6.5 and 14ms). At 20MHz, the relationship between T_2 and the inverse of temperature is linear for the three TEs studied with only slight differences between the slopes. It corresponds to a fast exchange regime across the whole temperature range. At 60MHz, the relationship between T_2 and $1/T$ is strongly impacted by the TE. T_2 varies linearly with $1/T$ for TE of 6.5 and 14ms between 40 and 25°C, but was almost constant for lower temperatures. At 100MHz, for TE of 6.5 and 14ms, T_2 decreased with $1/T$ until about 20°C, and increased for lower temperatures. For $TE=1\text{ms}$, at both 60 and 100MHz, T_2 has a poor sensitivity to temperature across the full range of temperatures investigated. This singular behavior is due to the fact that in the temperature range analyzed, for $TE=1\text{ms}$ the exchange regime changes from slow (5°C) to intermediate (40°C), as TE is respectively short and long comparing to $1/k_b$. The similar T_2 values for $TE=6.5\text{ms}$ and $TE=14\text{ms}$ at high temperatures at both 60 and 100MHz is explained by the long TE limit (Eq. 3). In fact, the increase in k_b with the temperature causes the midpoint of the dispersion curve to shift to higher TE^{-1} values (Fig. 1.B) and, consequently, to a widening of the plateau corresponding to the long echo times. For pH different from neutral, T_2 significantly increases and the relationship between T_2 and the inverse of temperature changes as can be observed for 60MHz and $TE=6.5\text{ms}$. Indeed, for $\text{pH}=6(8)$, T_2 varies with temperature as is observed

for pure liquids under Arrhenius's law [11], due to the strong increase in k_b leading to the fast exchange regime.

IMAGING EXPERIMENT AT 1.5T

This section describes the effects of chemical exchange on transverse relaxation parameters obtained experimentally using a MRI system operating at 1.5T (63.3MHz), representative of mid-strength magnetic field imagers and incorporating all the constraints associated with scanner specifications (inhomogeneities of B_1 and B_0 , imperfect refocusing pulses etc.). The experimental data were fitted using the Carver Richards model.

The transverse relaxation rates of pure water, fructose and glucose solutions measured at 8°C and at different echo times (6.5 to 20ms) are reported in Fig.3. The relaxation rate of water very slightly decreased with the echo time (less than 2% between 6.5 and 20ms). This can be attributed to several T_2 -reducing phenomena, caused by the diffusion of water molecules in the imaging gradients and RF pulse imperfections, which, in turn depend on TE in a complex way [24]. The mean magnetic field gradients caused by the inhomogeneities of the static magnetic field, intrinsic to the MRI system or produced by experimental device susceptibility were estimated experimentally at about 0.05mT/m. According to [25], this value is too low to impact significantly R_2 observed (less than 2.5×10^{-5} % of the T_2 value measured). R_2 of glucose and fructose solutions was modulated by TE where the pH was neutral, but varied only slightly for an acid pH (4.4). This difference in dispersion curves was due to the increase in k_b when the pH moves away from neutral (Eq.2). Where pH was acid, the midpoint value of the dispersion curves shifted to shorter echo times, and the plateau corresponding to the long echo times was reached more quickly [11]. At the same concentration level, R_2 of the glucose solution was higher than that of the fructose solution due to the greater chemical shift difference between the solute and water protons, in agreement with the numerical simulations shown in Fig. B2. The experimental data also confirmed the strong effect of pH on the relaxation rates of glucose and fructose solutions due to variations in k_b . For example, a decrease in pH from 7.0 to 4.4 induces a 32% decrease in R_2 (2.25 to $1.53s^{-1}$) in the case of the glucose solutions at TE=20ms. Note that a 50:50 solution of glucose and fructose at pH 4.4 (58g/L) had almost the same R_2 values as a glucose solution at half the concentration (29 g/L) with a neutral pH, confirming experimentally that variations in pH can considerably reduce the expected effects of sugar concentration on relaxation rates. Further, R_2 of the 50:50 fructose and glucose solution with a concentration of 29g/L at pH=4.4 was equal to the weighted R_2 average of the two pure sugar solutions at the same concentration and pH.

The dependence of R_2 on temperature (8-32°C) for TEs of 6.5 and 20ms is illustrated in Fig. 4. Accordingly to Fig. 3, TE had slight effect on R_2 for pure water or for solutions with an acid pH, resulting

in almost the same linear relationship between T_2 and inverse temperature. Conversely, for sugar solutions at neutral pH, this relationship was complex, with the decrease in T_2 with the temperature rise from 5 to 20°C, as predicted by the simulation (Fig. 2). Note that the same R_2 was measured for different temperatures, as shown for glucose at 8 and 24°C.

Figs.5 A and B show the experimental and fitted dispersion curves of 29g/L fructose and glucose pH-neutral aqueous solutions respectively, at 8, 12, 15, 20, 24 and 32°C. Since k_b varied with temperature and $\Delta\omega$ remained almost unchanged, the different exchange conditions were observed for both solutions. As temperature increased, the mid-point of the dispersion curves shifted toward higher TE^{-1} values due to the increase in k_b , resulting in decrease in variations in R_2 for the range of the TE analyzed. Moreover, due to the changes in the chemical exchange regime, the dispersion curves intersected for several values of TE, particularly in the case of the glucose solution that has a higher chemical shift than fructose. Consequently, depending on the TE used, the same or very closed R_2 values were measured at different temperatures. These results provide experimental evidence that chemical exchange effects on relaxation time of low-concentrated sugar solutions are significant in the narrow range of echo times accessible through MR imaging at a moderated field of 1.5T.

Estimation of the Carver-Richards parameters was possible for temperatures up to 20 and 24°C for fructose and glucose respectively. At higher temperatures, slight variations in R_2 prevented an accurate fit of the dispersion curves. At 8°C, estimated P_b values were 8.8×10^{-3} and 8.2×10^{-3} for fructose and glucose respectively. The slight deviation of the P_b from its theoretical value (7.6×10^{-3}) can be explained by the assumptions that exchange rates and chemical shifts were the same for all exchangeable protons of the sugar molecule that were adopted. For higher temperatures, P_b was fixed at the values obtained at 8°C, in order to reduce the number of variables and thereby allow a more accurate fit. The estimated exchange rates, chemical shifts and T_{2b} at different temperatures are reported in Table 1. The values of the chemical shift and k_b estimated from Carver Richard model were consistent with both the simulation and the literature [15, 26]. T_{2b} was the parameter with the highest estimate uncertainty, consistent with the fact that the variation in T_{2b} with temperature under Arrhenius's law [18] was rarely verified [22, 27, 28]. For $T > 20^\circ\text{C}$ for fructose and $T > 24^\circ\text{C}$ for glucose, k_b values were extrapolated following Eyring's law (Eq. 1) by slightly varying the values of the other parameters ($\Delta\omega$ and T_{2b}) around the mean values obtained from the adjustments at lower temperatures. A linear relationship between the exchange rate and the temperature was observed (Fig.6), according to what was expected from Eyring's relation (Eq. 1) and confirming the suitability of the estimated parameters. Moreover, the k_b values obtained by adjustment and extrapolation are of the same order of magnitude as the values previously reported for these sugar concentrations and temperatures [13, 18].

In conclusion, we have shown that the relaxation times of low-concentrate aqueous sugar solutions modeling the vacuolar water in fruit cells can be strongly modulated by the experimental conditions (echo time, magnetic field strength, temperature) as a result of chemical exchange, even for low and mid magnetic field strengths and for a narrow echo time range. This makes the interpretation of the evolution of bulk relaxation times during physical processes highly complex. We therefore recommend that all these variables should be taken into account before an interpretation of NMR/MRI relaxation time experiments is put forward and before comparison of results obtained under different experimental conditions. Indeed, it is clear that relaxation time measurements should be interpreted following detailed analysis of all possible parameters involved in the chemical exchange mechanism. It is important to note that several effects such as background gradients due to B_0 inhomogeneities, imaging gradients or RF pulse imperfections (for MRI) will lead to deviations of dispersion curves from ideality. In the present case, these phenomena had a minor impact in the range of the echo time studied. The effects of magnetic susceptibility on the impact of TE on relaxation times, which are known to be highly significant at high field strengths, should also be taken into account. Additionally to the impact of the chemical exchange of water protons with macromolecules on bulk relaxation, the proton exchanges with solid surfaces should also be taken into account, as well as the possible variations in diffusional exchanges of water molecules between compartments that can result from the process under investigation. Nevertheless, we have demonstrated that the appropriate choice of experimental conditions offers a powerful strategy to maximize the effects of sugar concentration or pH variations on transverse relaxation in vacuolar liquid, enabling monitoring of these parameters. Moreover, in order to increase the level of information on the water status in plant tissues accessible by TD NMR and MRI, T_2 measurements can be coupled with other parameters such as the self-diffusion coefficient. This could be useful to the analysis of processes such as fruit ripening where changes occur simultaneously in water content and in the chemical reactions that involve the transformation of sugars and organic acids (potentially associated with changes in pH). The combination of relaxation and diffusion measurements provides a way to monitor these effects independently.

ACKNOWLEDGMENTS

This work was in part funded by the Région Bretagne. The authors would like to thank Guylaine Collewet (UR OPAALE, INRAE) for her help in estimating the parameters of the Carver-Richards model from the experimental dispersion curves. We are most grateful to the PRISM core facility (Rennes-Angers, France) for its technical support, and the GIS Biogenouest.

APPENDIX A

The effects of chemical exchange between two spin species (a, b) in homogeneous sugar systems can be estimated using the theoretical dispersion curves (variation of relaxation rate with interpulse spacing of the Carr-Purcell-Meiboom-Gill (CPMG) pulse sequence) provided by the Carver and Richard's equations and corrected by Hills [12, 13]:

- $\frac{1}{T_2} = -\frac{1}{TE} \ln \lambda_1$
- $\ln \lambda_1 = -TE \frac{\alpha_+}{2} + \ln \left[\sqrt{D_+ \cdot \cosh^2 \xi - D_- \cdot \cos^2 \eta} + \sqrt{D_+ \cdot \sinh^2 \xi + D_- \cdot \sin^2 \eta} \right]$

with:

- TE : echo time (time between two 180° RF pulses)
- $\alpha_+ = \frac{1}{T_{2a}} + \frac{1}{T_{2b}} + k_a + k_b$
- $\alpha_- = \frac{1}{T_{2a}} - \frac{1}{T_{2b}} + k_a - k_b$
- T_{2a} and T_{2b} : transverse relaxation times of the water protons and the exchangeable protons of the solute respectively.
- τ_a and τ_b : lifetimes of states *a* and *b* respectively.
- $k_a = \frac{1}{\tau_a}$ and $k_b = \frac{1}{\tau_b}$: exchange rates at sites *a* and *b* respectively. ($k_a = \frac{P_b}{P_a} k_b$)
- P_a and P_b : fractions of the total proton population at sites *a* and *b* respectively.
($P_a = 1 - P_b$) and $P_b = \frac{\text{number of exchangeable protons of the solute}}{\text{number of protons exchangeable in the solution (solvent + solute)}}$
- $2D_+ = 1 + \frac{\psi + 2\Delta\omega^2}{\sqrt{(\psi^2 + \zeta^2)}}$
- $2D_- = -1 + \frac{\psi + 2\Delta\omega^2}{\sqrt{(\psi^2 + \zeta^2)}}$
- $\Delta\omega = \omega_b - \omega_a$: Chemical shift difference given in units of radial frequency rad s⁻¹.
- $\psi = \alpha_-^2 - \Delta\omega^2 + 4k_a k_b$
- $\zeta = 2\Delta\omega \cdot \alpha_-$
- $\xi = \left(\frac{TE}{2\sqrt{2}} \right) \left[\psi + (\psi^2 + \zeta^2)^{\frac{1}{2}} \right]^{\frac{1}{2}}$
- $\eta = \left(\frac{TE}{2\sqrt{2}} \right) \left[-\psi + (\psi^2 + \zeta^2)^{\frac{1}{2}} \right]^{\frac{1}{2}}$

The chemical shift $\Delta\omega$ is given in units of radial frequency (rad s⁻¹): $\Delta\omega = 2\pi \times B_0 \times \delta\omega$, where $\delta\omega$ is the chemical shift difference between the two sites *a* and *b* in ppm.

Note that for the cases of higher values of P_b , a model that take into account exchange during signal detection and enables an improved theoretical description of the CPMG experiment has been proposed by [29].

APPENDIX B

Effects of sugar concentration

Fig. B1 illustrates the impact of the solute concentration (5 to 60g/L, water content from 99.5 to 94.1%) on the relaxation rate for different magnetic field strengths (20, 60 and 100MHz) and echo times (1, 6.5 and 14ms). The simulated data correspond to glucose at low temperature (5°C) and neutral pH, with $k_b=300s^{-1}$; which correspond to an intermediate exchange regime. As expected for the dilute systems, the relation between $1/T_2$ and concentration is linear [30]. The slope of the linear relationship, and therefore the sensitivity of the R_2 to the solution concentration, depends on both magnetic field strength and TE. The sensitivity of R_2 to concentration and B_0 at long echo times ($1/TE \ll k_b/2$) is consistent with the Swift-Connick equations (Eq.3 and 4), demonstrating that in these conditions R_2 depends upon $\Delta\omega$ in addition to T_{2a} , k_b , P_b and T_{2b} . The present results show that the sensitivity of R_2 to concentration significantly increases with B_0 even for low and mid magnetic field strength and for very low concentration range, supplementing the results obtained at high magnetic field strengths [31].

Effects of sugar structure

Because the effects of chemical exchange on the transverse relaxation of the homogeneous sugar solution depend on the absolute frequency difference between water and sugar protons (expressed in $rad.s^{-1}$), dephasing is modulated by both magnetic field strength and sugar type. This is illustrated in Fig. B2 by the particular case of fructose and glucose that are characterized by the same molar mass and the same number of exchangeable protons, but the protons in the hydroxyl groups shifted by 0.8 and 1.2ppm from water protons [15, 26] respectively. At 20MHz, variations in relaxation times are only slightly impacted by the nature of the sugar, as the effect of the chemical shift is weak. This effect increases with the magnetic field strength leading in large differences in R_2 values for glucose and fructose solutions for the highest concentrations analyzed at 60 and 100MHz. The impact of sugar type on R_2 should therefore be taken into account when the processes involving sugar transformations (i. e. sucrose hydrolysis) such as fruit development and ripening are studied.

Effects of pH

Fig B3 depicts the impact of the pH value on the relationship between R_2 and solute concentrations at 20, 60 and 100MHz, simulated using Eq. 2. The autoprotolysis constant for water (K_w) was fixed at 10^{-14} [32] and the constants k_1 and k_2 were fixed at $6 \times 10^8 dm^3.mol^{-1}.s^{-1}$ [11, 33]. It can be observed that the sensitivity of R_2 to concentration strongly depend on the pH. At 60MHz and for a very low solute concentration of 20g/L, a variation in pH from 7 to 5 leads to a large decrease in R_2 from 1.303 to $0.817s^{-1}$ (T_2 of 767 and 1224ms), which at neutral pH would require a decrease in

concentration from 20 to 5g/L. This phenomenon is explained by the fact that when pH values move away from neutral, the value of k_b increases dramatically [11], leading in some cases to the transition between fast and slow exchange regimes. It is therefore essential to control the pH value when relaxation times are used to estimate changes in solute concentration in plant tissues.

REFERENCES

- [1] H. Van As, Intact plant MRI for the study of cell water relations, membrane permeability, cell-to-cell and long distance water transport, *Journal of Experimental Botany*, 58 (2006) 743-756.
- [2] C.J. Clark, L.N. Drummond, J. Mac Fall, Quantitative NMR imaging of kiwifruit (*actinidia deliciosa*) during growth and ripening, *Journal of Science and Food Agriculture*, 78 (1998) 349-358.
- [3] M. Musse, L. De Franceschi, M. Cambert, C. Sorin, F. Le Caherec, A. Burel, A. Bouchereau, F. Mariette, L. Leport, Structural changes in senescing oilseed rape leaves at tissue and subcellular levels monitored by nuclear magnetic resonance relaxometry through water status, *Plant physiology*, 163 (2013) 392-406.
- [4] G. Winisdorffer, M. Musse, S. Quellec, A. Barbacci, S.L. Gall, F. Mariette, M. Lahaye, Analysis of the dynamic mechanical properties of apple tissue and relationships with the intracellular water status, gas distribution, histological properties and chemical composition, *Postharvest Biology and Technology*, 104 (2015) 1-16.
- [5] B.P. Hills, B. Remigereau, NMR studies of changes in subcellular water compartmentation in parenchyma apple tissue during drying and freezing, *Int J Food Sci Technol*, 32 (1997).
- [6] F. Mariette, S. Rodriguez, T. Lucas, P. Marchal, Influence de la déshydratation sur la répartition cellulaire de l'eau étudiée par relaxation RMN, in: *Les produits alimentaires et l'eau*, Agoral 99, Edition Tec & Doc, Nantes, 1999, pp. 417-422.
- [7] F. Xu, X. Jin, L. Zhang, X.D. Chen, Investigation on water status and distribution in broccoli and the effects of drying on water status using NMR and MRI methods, *Food Research International*, 96 (2017) 191-197.
- [8] M. Musse, M. Cambert, F. Mariette, NMR study of water distribution inside tomato cells: effects of water stress, *Applied Magnetic Resonance*, 38 (2010) 455-469.
- [9] A. Raffo, R. Gianferri, R. Barbieri, E. Brosio, Ripening of banana fruit monitored by water relaxation and diffusion ¹H-NMR measurements, *Food Chemistry*, 89 (2005) 149-158.
- [10] M. Mortensen, A.K. Thybo, H.C. Bertram, H.J. Andersen, S.B. Engelsen, Cooking effects on water distribution in potatoes using nuclear magnetic resonance relaxation, *Journal of agricultural and food chemistry*, 53 (2005) 5976-5981.
- [11] B.P. Hills, Nuclear magnetic resonance relaxation studies of proton exchange in methanol–water mixtures, *Journal of the Chemical Society, Faraday Transactions*, 86 (1990) 481-487.
- [12] J. Carver, R. Richards, A general two-site solution for the chemical exchange produced dependence of T₂ upon the Carr-Purcell pulse separation, *Journal of Magnetic Resonance* (1969), 6 (1972) 89-105.
- [13] B. Hills, K. Wright, P.S. Belton, Proton NMR studies of chemical and diffusive exchange in carbohydrate systems, *Molecular Physics*, 67 (1989) 1309-1326.
- [14] B. Hills, S. Duce, The influence of chemical and diffusive exchange on water proton transverse relaxation in plant tissues, *Magnetic resonance imaging*, 8 (1990) 321-331.
- [15] J.M. Harvey, M.C. Symons, The hydration of monosaccharides—an NMR study, *Journal of Solution Chemistry*, 7 (1978) 571-586.
- [16] H. Eyring, The activated complex in chemical reactions, *The Journal of Chemical Physics*, 3 (1935) 107-115.

- [17] B. Hills, Multinuclear NMR studies of water in solutions of simple carbohydrates. I. Proton and deuterium relaxation, *Molecular physics*, 72 (1991) 1099-1121.
- [18] D. Fabri, M.A. Williams, T.K. Halstead, Water T2 relaxation in sugar solutions, *Carbohydrate research*, 340 (2005) 889-905.
- [19] H. Adriaensen, M. Musse, S. Quellec, A. Vignaud, M. Cambert, F. Mariette, MSE-MRI sequence optimisation for measurement of bi-and tri-exponential T2 relaxation in a phantom and fruit, *Magnetic resonance imaging*, 31 (2013) 1677-1689.
- [20] J.M. Bonny, M. Zanca, J.Y. Boire, A. Veyre, T2 maximum likelihood estimation from multiple spin - echo magnitude images, *Magnetic resonance in medicine*, 36 (1996) 287-293.
- [21] E.L. Kovrigin, J.G. Kempf, M.J. Grey, J.P. Loria, Faithful estimation of dynamics parameters from CPMG relaxation dispersion measurements, *Journal of magnetic resonance*, 180 (2006) 93-104.
- [22] B. Hills, *Magnetic resonance imaging in food science*, (1998).
- [23] T.J. Swift, R.E. Connick, NMR - relaxation mechanisms of O17 in aqueous solutions of paramagnetic cations and the lifetime of water molecules in the first coordination sphere, *The Journal of Chemical Physics*, 37 (1962) 307-320.
- [24] H. Adriaensen, M. Musse, S. Quellec, A. Vignaud, M. Cambert, F. Mariette, MSE-MRI sequence optimisation for measurement of bi- and tri-exponential T2 relaxation in a phantom and fruit., *Magn Reson Imaging*, 31 (2013) 1677-1689.
- [25] H.Y. Carr, E.M. Purcell, Effects of Diffusion on Free Precession in Nuclear Magnetic Resonance experiments, *Phys. Rev.*, 94 (1954) 630-638.
- [26] M. Symons, J. Benbow, J. Harvey, Hydroxyl-proton resonance shifts for a range of aqueous sugar solutions, *Carbohydrate Research*, 83 (1980) 9-20.
- [27] K. Szutkowski, P. Stilbs, S. Jurga, Proton chemical exchange in aqueous solutions of dodecylammonium chloride: Effects of micellar aggregation, *The Journal of Physical Chemistry C*, 111 (2007) 15613-15619.
- [28] B. Hills, K. Nott, NMR studies of water compartmentation in carrot parenchyma tissue during drying and freezing, *Applied Magnetic Resonance*, 17 (1999) 521-535.
- [29] A.J. Baldwin, An exact solution for R2, eff in CPMG experiments in the case of two site chemical exchange, *Journal of magnetic resonance*, 244 (2014) 114-124.
- [30] B. Hills, S. Takacs, P. Belton, The effects of proteins on the proton NMR transverse relaxation times of water: I. Native bovine serum albumin, *Molecular Physics*, 67 (1989) 903-918.
- [31] N.N. Yadav, J. Xu, A. Bar - Shir, Q. Qin, K.W. Chan, K. Grgac, W. Li, M.T. McMahon, P.C. van Zijl, Natural D - glucose as a biodegradable MRI relaxation agent, *Magnetic resonance in medicine*, 72 (2014) 823-828.
- [32] P. Muller, Glossary of terms used in physical organic chemistry (IUPAC Recommendations 1994), *Pure and Applied Chemistry*, 66 (1994) 1077-1184.
- [33] S. Aime, R. Nano, M. Grandi, A new class of contrast agents for magnetic resonance imaging based on selective reduction of water-T2 by chemical exchange, *Investigative radiology*, 23 (1988) S267-270.

CAPTIONS

Table 1. Values of k_b , $\Delta\omega$ and T_{2b} extracted from the fits of the Carver-Richard model presented in Fig. 5 A and B, except for the values marked with an asterisk (*) which were obtained by extrapolation.

Fig. 1: Relaxation dispersion curves simulated for 60g/L ($P_b=0.015$) glucose solution ($\Delta\omega=1.2\text{ppm}$ and $T_{2b}=50\text{ms}$) and for different magnetic field strengths (8; 20; 60; 80; 100; 200MHz). 100% of the hydroxyl protons are assumed to be accessible to exchange and have the same chemical shift. A corresponds to 5°C with $k_b=300\text{s}^{-1}$ and $T_{2a}=1.5\text{s}$ and B corresponds to 20°C with $k_b=1000\text{s}^{-1}$ and $T_{2a}=1.5\text{s}$. The shaded area indicates the range of echo time values usually accessible through both MRI and NMR, echo times to the left of this zone are accessible only through MRI and echo times to the right of this zone only through NMR.

Fig. 2 : Numerical simulation of the relationship between T_2 of 20g/L glucose solution and temperature (5–40°C, 8 values equally spaced) at different field strengths (20, 60 and 100MHz) and echo times (1.0, 6.5 and 14ms). Parameters values: $P_b=0.005$; $\Delta\omega=1.2\text{ppm}$; $T_{2b}=50\text{ms}$; $T_{2a}=1.5, 1.7, 1.8, 2.0, 2.2, 2.3, 2.5$ and 2.7s ; $k_b= 300, 456, 687, 1020, 1495, 2164, 3096$ and 4380s^{-1} ; $\text{pH}=7$. For 60MHz and $\text{TE}=6.5\text{ms}$, T_2 dependence on temperature is also shown for $\text{pH}=6(8)$.

Fig. 3 : Transverse relaxation dispersion (6.5 – 20ms) for 29 g/L glucose (◆- pH 7; ▲- pH 4.4) and fructose (◆- pH 7; ▲- pH 4.4) solutions and pure water (●) observed by MRI at 1.5T (63MHz) with a MSE sequence ($\text{TE}=6.5\text{ms}$ $\text{TR}=10\text{s}$, 256 echoes) at 8°C.

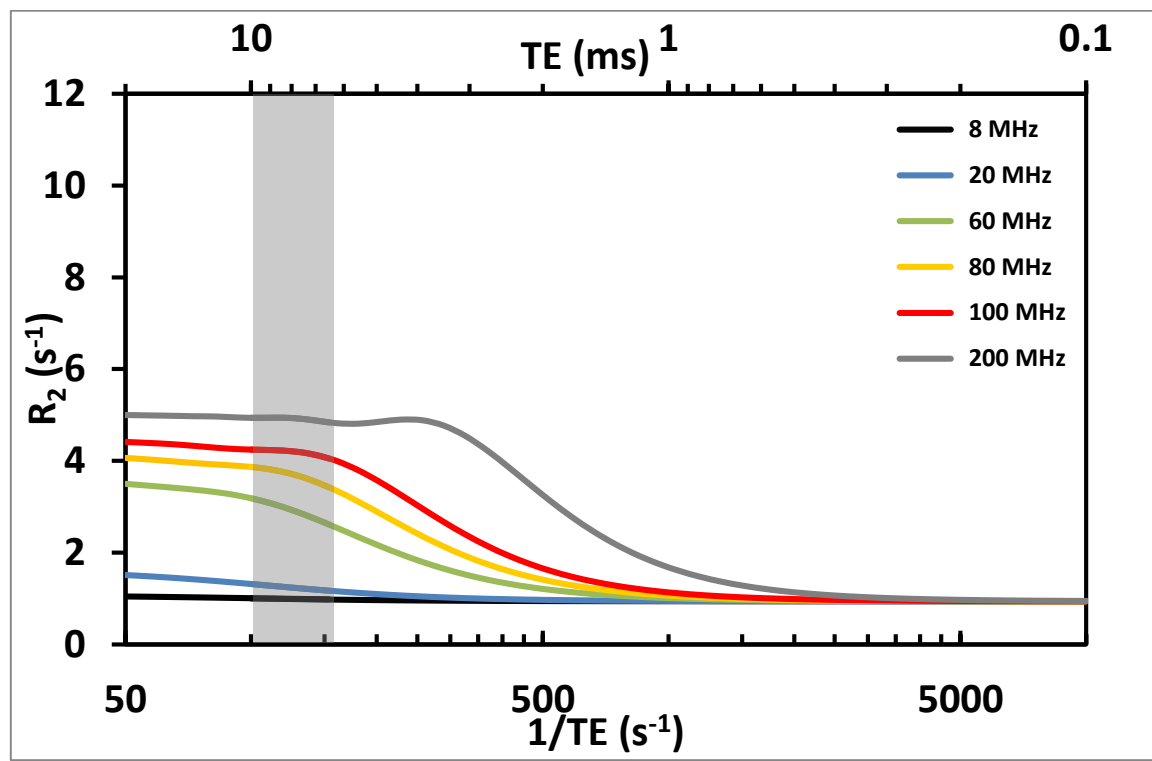
Fig. 4 : Transverse relaxation for fructose 29 g/L (✕- pH 7; ■-pH 4.4) and glucose (✕-pH 7; ■- pH 4.4) aqueous solutions and pure water (●), observed by MRI at 1.5T (63MHz) with a MSE sequence ($\text{TR}=10\text{s}$, 256 echoes) at 8°C. For the sugar solutions, (✕) and (■) symbols correspond to $\text{TE}=6.5\text{ms}$, (◆) and (▲) symbols correspond to $\text{TE}=20\text{ms}$. For water, grey and black symbols correspond to $\text{TE}=6.5\text{ms}$ and $\text{TE}=20\text{ms}$ respectively.

Fig. 5 A – Transverse relaxation dispersion curves for 29g/L fructose (A) and glucose (B) aqueous solutions at neutral pH, observed by MRI at 1.5T (63MHz) with MSE sequence ($\text{TE}=6.5\text{ms}$, $\text{TR}=10\text{s}$, 256 echoes) at 8 (▲), 12 (◆), 15 (■), 20 (●), 24 (◻), 28 (✕) and 32°C (⊕) °C. Solid lines are least square fits of the Carver-Richard model (Appendix A) to the experimental data (symbols) and dashed lines are extrapolations. For fitting, P_b of fructose (A) and glucose (B) was fixed at 8.8×10^{-3} and 8.2×10^{-3} , respectively.

Temperature (°C)	Exchange Rate (s ⁻¹)		Chemical shift difference (ppm)		T _{2b} (s)	
	Fructose (29.4 g/L)	Glucose (28.8 g/L)	Fructose (29.4 g/L)	Glucose (28.8 g/L)	Fructose (29.4 g/L)	Glucose (28.8 g/L)
8.2	346 ± 32	297 ± 9	0.86 ± 0.04	1.23 ± 0.02	0.047 ± 0.014	0.025 ± 0.002
11.7	430 ± 55	467 ± 23	0.85 ± 0.03	1.28 ± 0.01	0.037 ± 0.015	0.066 ± 0.015
15.4	404 ± 68	555 ± 36	0.75 ± 0.02	1.32 ± 0.01	0.019 ± 0.005	0.046 ± 0.013
19.6	645 ± 396	537 ± 61	0.74 ± 0.27	1.24 ± 0.01	0.029 ± 0.043	0.018 ± 0.003
23.6	830*	568 ± 66	0.72*	1.06 ± 0.02	0.035*	0.011 ± 0.002
27.8	1050*	1175*	0.75*	1.2*	0.065*	0.03*
31.9	1275*	1550*	0.75*	1.2*	0.06*	0.035*

Figure 1

A



B

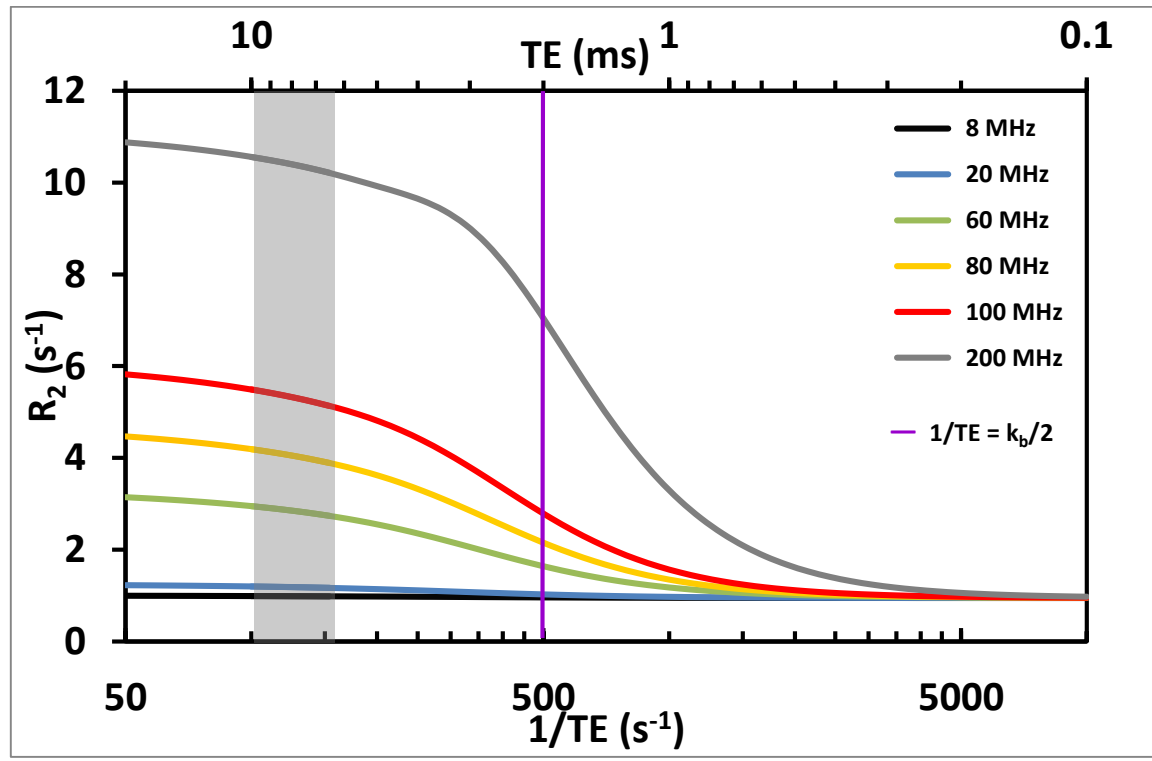


Figure 2

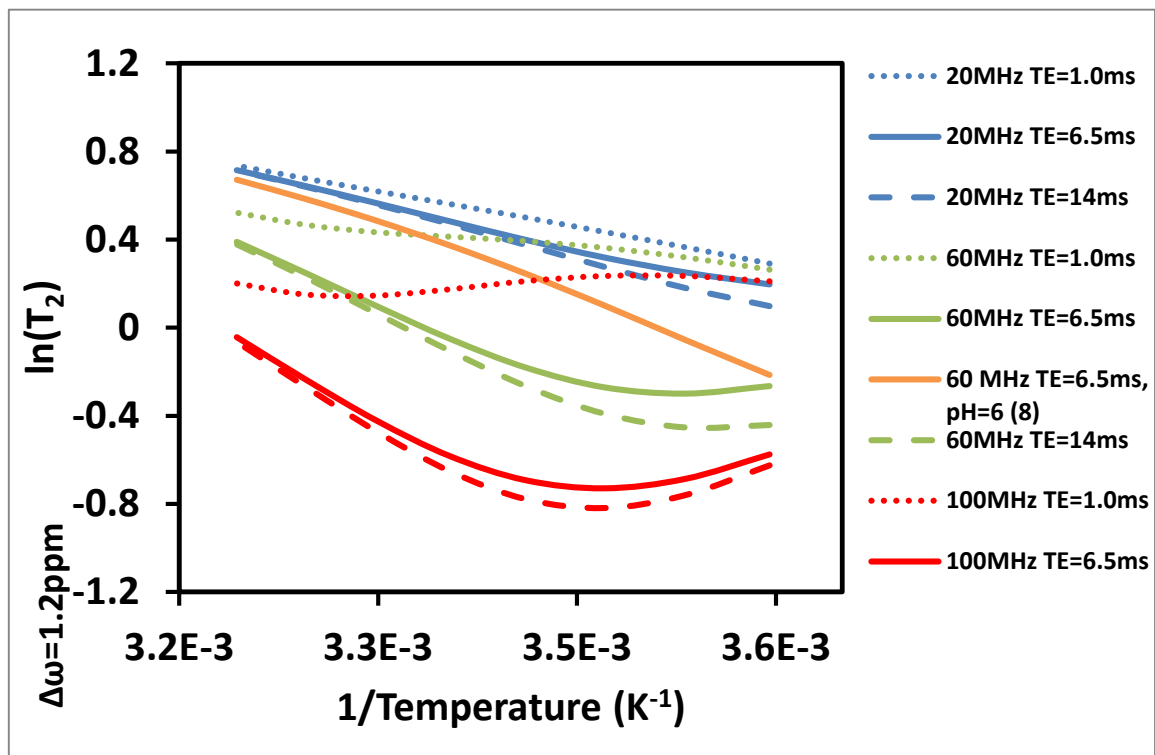


Figure 3

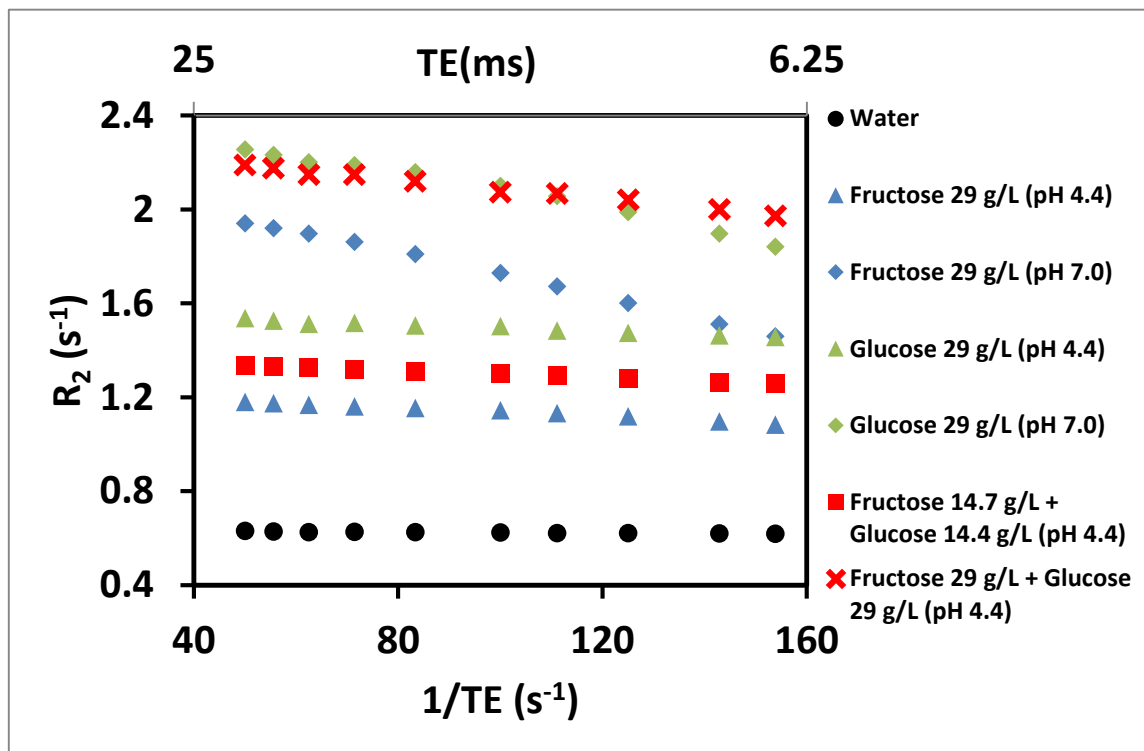


Figure 4

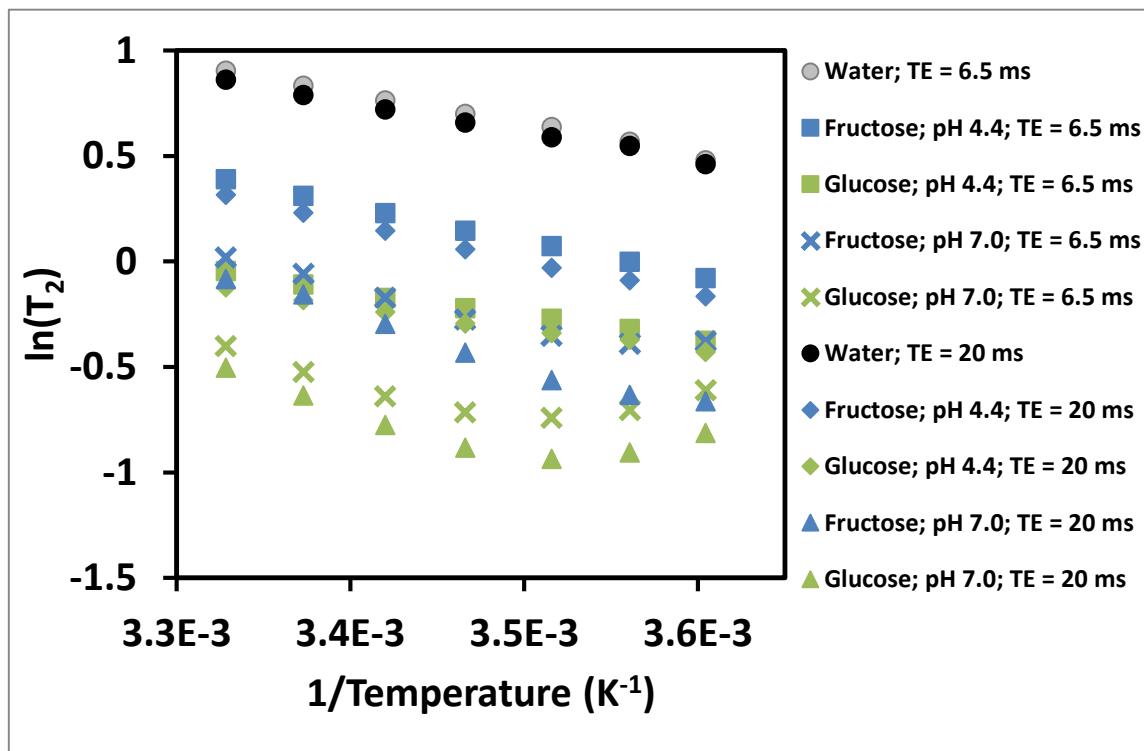
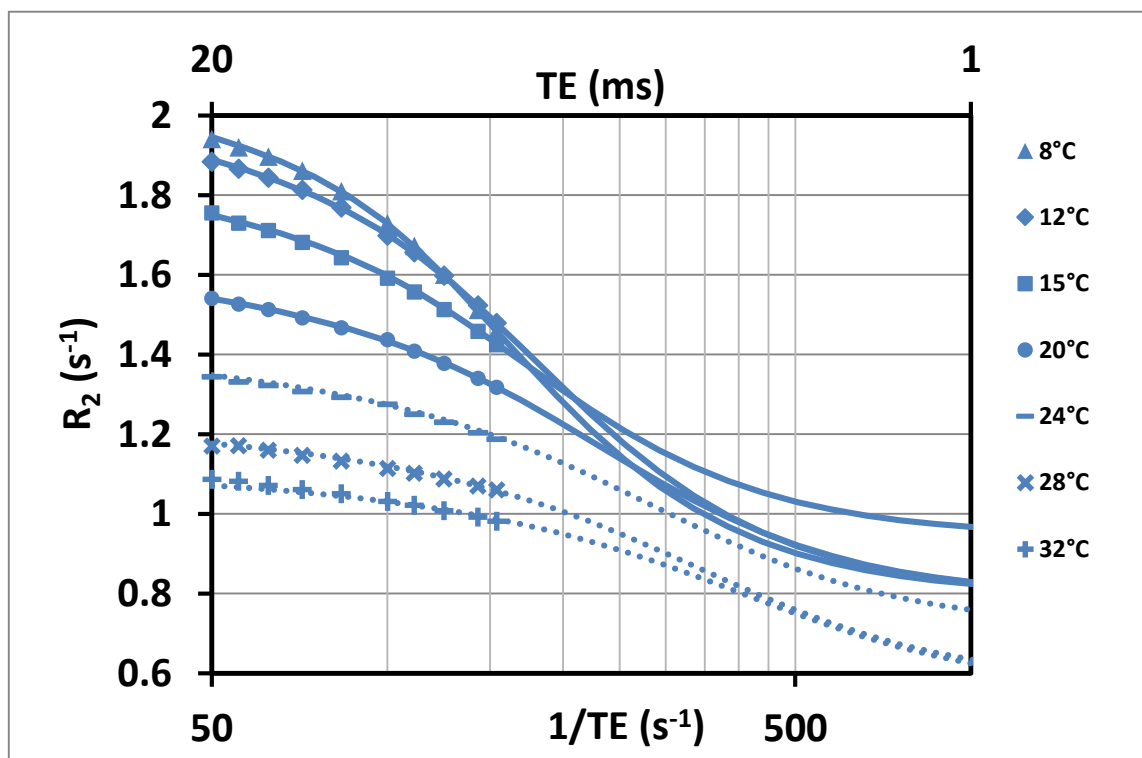


Figure 5

A



B

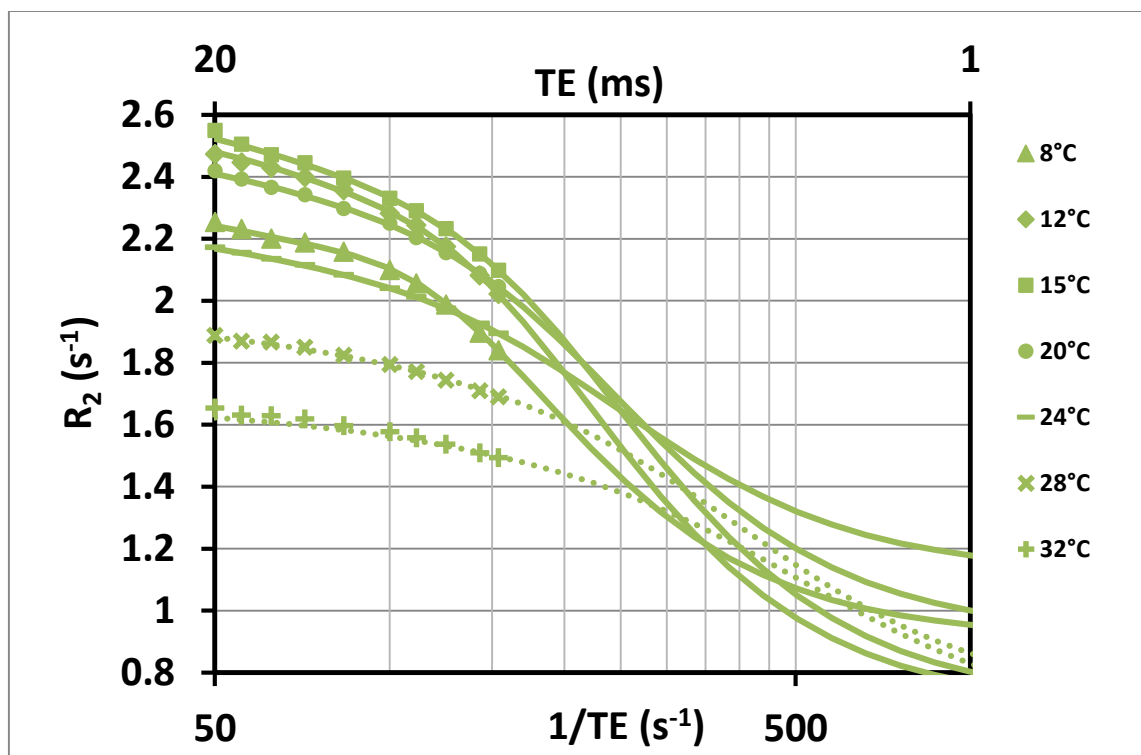


Figure 6

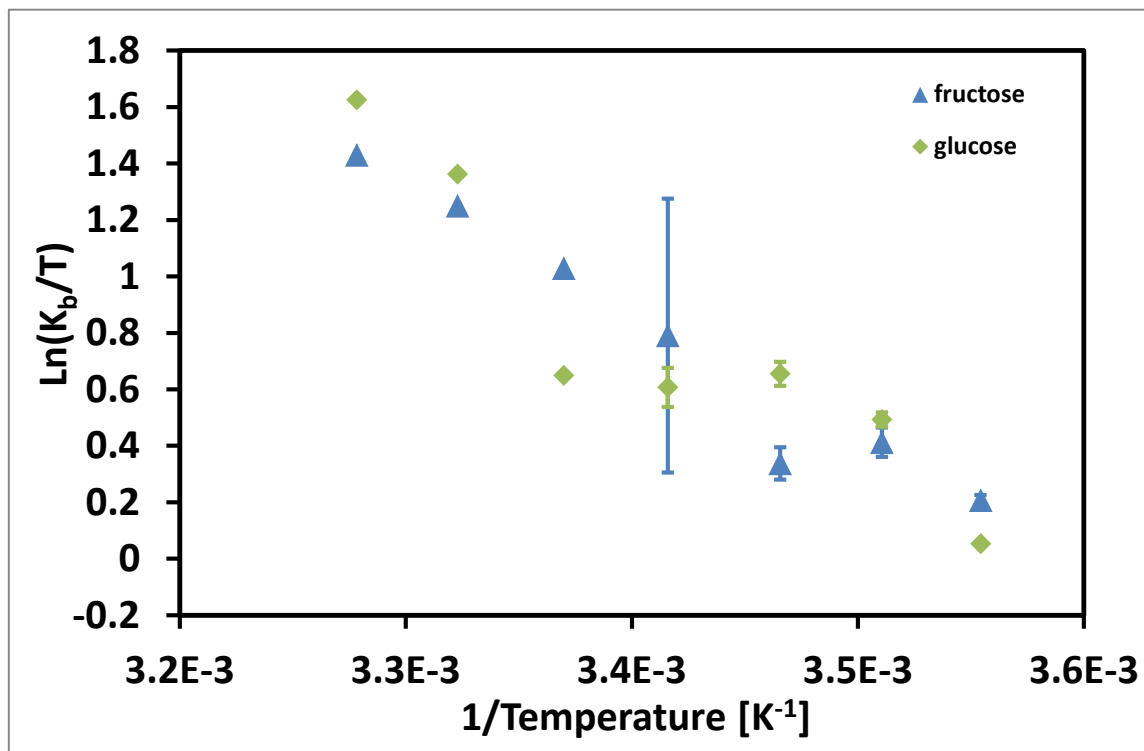


Figure B1

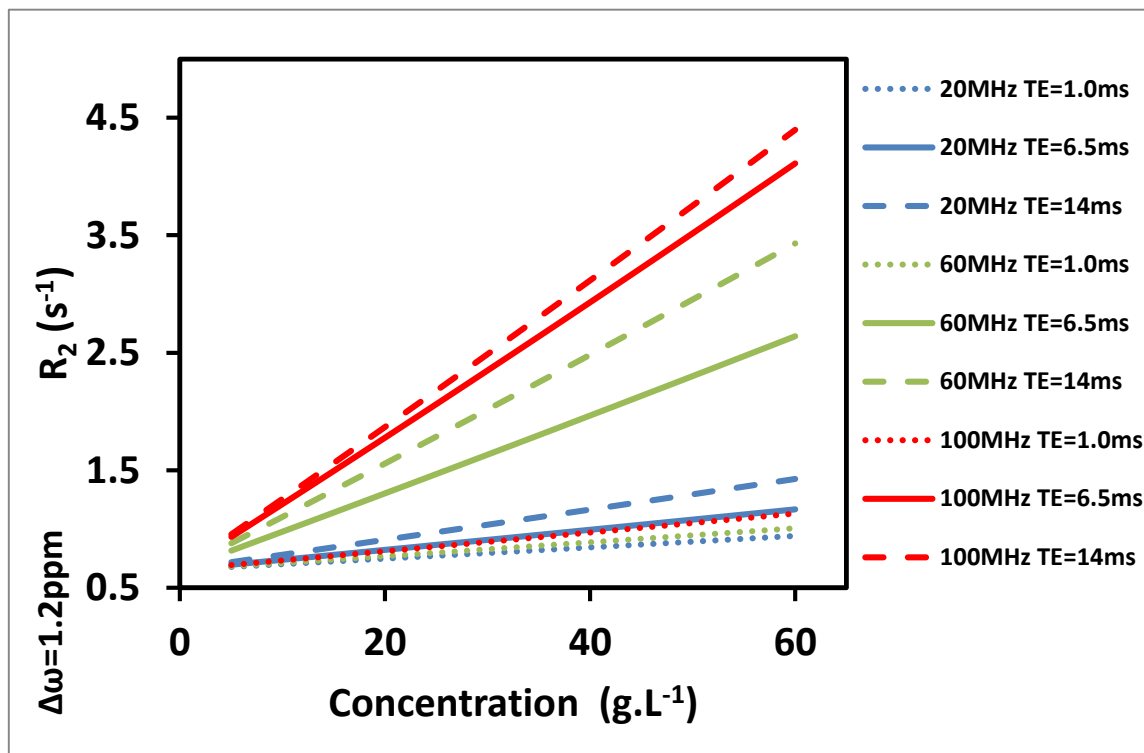


Figure B2

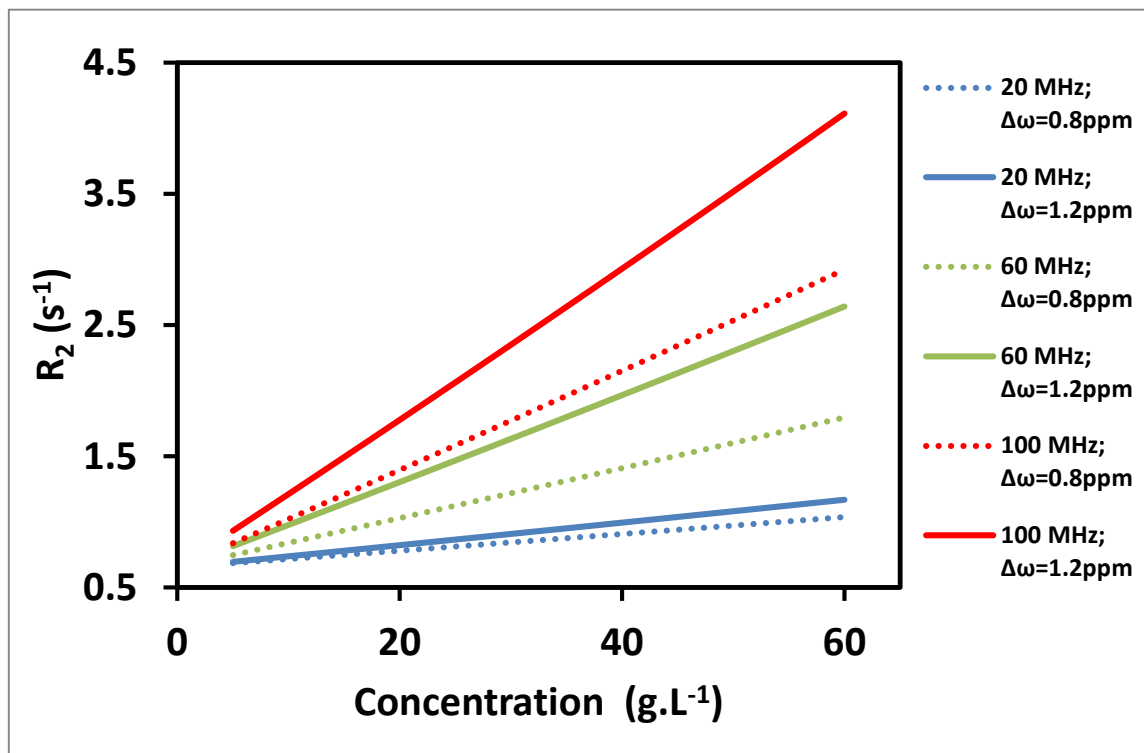


Figure B3

